Journal of Asian Concrete Federation
Vol. 11, No. 4, pp. 45-57, December 2025
ISSN 2465-7964/ eISSN 2465-7972
DOI http://dx.doi.org/10.18702/acf.2025.11.4.45

Technical Paper

Effect of graphene dispersion methods on mechanical and electrical properties of ultra–low–w/b cement pastes

Dengwu Jiao*, Shuo Wang, Feng Hu

(Received: 29-Oct-2025; Revised: 21-Nov-2025; Accepted: 13-Dec-2025; Published online: 27-Dec-2025)

Abstract: This study investigates the influence of different dispersion methods of graphene nanoplatelets (GNPs) on the fluidity, mechanical, electrical, and microstructural properties of cement pastes with ultra-low water-to-binder (w/b) ratio of 0.18. Five dispersion strategies including ultrasonication (30 min and 60 min), mechanical stirring, and hybrid dispersion with silica fume (5% and 10%) were evaluated. Results reveal that extended ultrasonication for 60 min slightly reduced the initial fluidity but produced more stable time-dependent flow behavior due to the increased water adsorption on well-dispersed GNPs. Compared to the reference paste, the paste mixture after ultrasonication treatment for 60 min achieved the highest flexural and compressive strengths, as well as the most reduced electrical resistivity. This is possibly due to the fact that uniform GNP dispersion promotes crack bridging, nucleation of hydration products, and microstructural densification. Conversely, silica fume incorporation markedly improved early compressive strength through pozzolanic reactions and particle packing but significantly increased the electrical resistivity by disrupting conductive pathways. The findings highlight that dispersion efficiency is an important factor in maximizing the multifunctional potential of GNPs-containing cementitious composites, offering valuable insights for designing the next-generation high-performance self-sensing materials.

Keywords: Graphene nanoplatelets; Ultra-low-w/b paste; Dispersion; Mechanical properties; Electrical conductivity

1. Introduction

Concrete remains the foundational civil engineering material of modern infrastructure due to its outstanding compressive strength, fire resistance, and long-term durability [1]. However, conventional cement-based materials inherently exhibit quasi-brittle behavior, limited tensile strength, and poor toughness, leading to the formation of cracks that compromise the structural integrity and increase maintenance costs [2, 3]. To overcome this challenge, nanotechnology has emerged as a promising strategy to enhance the mechanical and functional performance of concrete [4, 5]. Among these, graphene nanoplatelets (GNPs) have attracted extensive attention owing to their exceptional mechanical, electrical, and thermal properties [6, 7], which offer unique opportunities to produce functional and high-performance cementitious composites.

Despite the potential of GNPs, its poor dispersibility in aqueous and cementitious systems remains a critical limitation. The strong van der Waals attractions, high surface energy, and inherent hydrophobicity of GNPs promote agglomeration, hindering their uniform distribution within the matrix and limiting their reinforcing efficiency [8, 9]. Achieving homogeneous and stable graphene dispersion is thus essential for realizing its multifunctional benefits in cement-based materials. In this context, extensive research has been

*Corresponding author **Dengwu Jiao,** *Department of Architecture and Civil Engineering, City University of Hong Kong, Hong Kong, China.*
E–mail: dengwu.jiao@cityu.edu.hk
Shuo Wang, *Department of Architecture and Civil Engineering, City University of Hong Kong, Hong Kong, China*
Feng Hu, *Department of Architecture and Civil Engineering, City University of Hong Kong, Hong Kong, China*

devoted to optimizing graphene dispersion strategies. Qamar et al. [10] categorized the primary approaches into physical and surface treatments (including covalent and non-covalent methods), while subsequent studies [11, 12] demonstrated that the combination of polycarboxylate superplasticizers with ultrasonic or high-shear mixing can significantly improve the dispersion stability. Other researchers [13-15] have shown that prolonged ultrasonication and hybrid dispersion techniques enhance both the distribution of GNPs and the mechanical performance of the cementitious composites.

Nevertheless, most existing studies have focused on conventional cementitious systems with water-to-binder (w/b) ratios ranging from 0.3 to 0.5, where sufficient fluidity facilitates the effective dispersion of nanoparticles [16]. In contrast, ultra-low w/b cement pastes, which form the basis of ultra-high performance concrete (UHPC), pose significant challenges due to their high viscosity and restricted workability, which intensify the agglomeration tendency of nanoparticles [17, 18]. Given the growing importance of UHPC in critical building structure and infrastructure applications, where superior strength, durability, and multifunctionality are required [19-21], a deep understanding the interaction between GNPs dispersion behavior and the microstructure of low-w/b matrix has becomes essential. In addition, the presence of ultra-fine solid particles in UHPC such as silica fume may affect the effectiveness of graphene dispersion [22, 23]. However, there is limited insight into how dispersion strategies affect the rheological, mechanical, and electrical properties of such dense cementitious systems.

To address the research gap, this study prepares cement pastes with GNPs at an ultra-low w/b of 0.18, typical for UHPC [24, 25]. Different dispersion techniques, including mechanical stirring, ultrasonic dispersion at varying durations, and hybrid dispersion with silica fume, are evaluated. Their effects on fluidity, flexural and compressive strengths, electrical conductivity, and microstructural development are analyzed. A comparative understanding of relationships between GNPs dispersion and paste performance within a dense matrix system is provided. The insights gained hopefully offer a pathway toward the design of high-performance, durable, and intelligent concrete materials for advanced structural and smart infrastructure applications.

2. Experimental program

2.1 Materials

This study employed CEM I 52.5 N Portland cement from Green Island Cement Company, with the chemical composition presented in Table 1. Few-layer graphene nanoplatelets (GNPs) were used, characterized by a bulk density of 0.01–0.02 g/mL, a thickness of less than 1 nm, a median particle size (D_{50}) of 7–12 μm, and high purity. The physical properties of the GNPs, as provided by the manufacturer, are summarized in Table 2. Compared with multilayer graphene, the utilized GNPs exhibit a lower density, a more uniform morphology, reduced agglomeration, and improved dispersibility. A polycarboxylate-based superplasticizer powder (SP, Shanghai Chenqi Chemical Technology Co., Ltd.) was used. A silica fume (SF) with SiO_2 content of 96.2%, a mean particle diameter of 0.1–0.3 μm, and a specific surface area of approximately 19.1 m^2/g was utilized. Tap water was used for mixing.

Table 1 Chemical composition of the cement (% by mass).

Material	SiO_2	Fe_2O_3	Al_2O_3	CaO	MgO
Portland Cement	20.7	3.2	6.3	65.6	1.2

Table 2 Physical properties of the GNPs.

Diameter(μm)	Thickness(nm)	Layers	Monolayer ratio (%)	Purity (wt%)	Specific surface area(m^2/g)
7.0-12.0	<1	1-3	>80	99	50-200

2.2 Mix proportion and sample preparation

To identify the optimal mix proportion, cement pastes with w/b ratio of 0.18, SP dosages of 1.5% or 1.7%, and GNP contents ranging from 0% to 0.1% were prepared. Based on the preliminary fluidity results, the mixture containing 0.05% GNPs and 1.5% SP demonstrated superior workability. Consequently, this formulation was selected as the reference mixture

for subsequent investigations.

To evaluate the effects of GNP dispersion on the performance of cement paste with GNPs at low w/b ratios, three dispersion methods were examined, including ultrasonic dispersion, mechanical stirring, and hybrid dispersion with silica fume. The overall experimental design is illustrated in Fig. 1, and the detailed mix proportions are presented in Table 3.

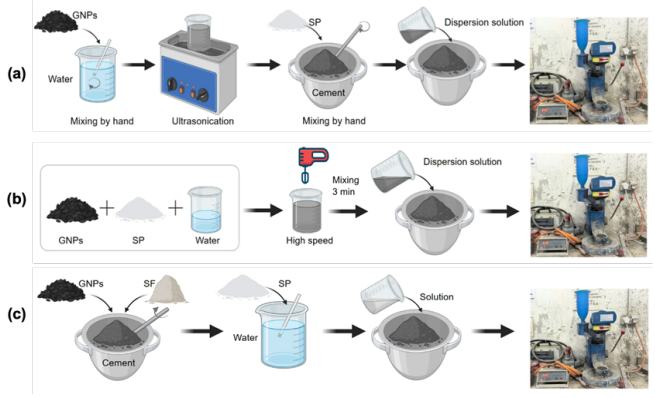

Fig. 1 Dispersion techniques used in this study. (a) ultrasonic dispersion, (b) mechanical stirring, and (c) hybrid dispersion with silica fume.

Table 3 Mixture proportions of the prepared cement pastes.

Mix	Cement (g)	Water (g)	GNPs (g)	SP (g)	SF (g)
Ref	2500.00	450	0	37.5	0
30min-Ult	2498.75	450	1.25	37.5	0
60min-Ult	2498.75	450	1.25	37.5	0
Mechanical stirring	2498.75	450	1.25	37.5	0
5%SF	2373.75	450	1.25	37.5	125
10%SF	2248.75	450	1.25	37.5	250

(1) Ultrasonic dispersion method

Ultrasonication of GNPs in water was performed at 25°C, and two treatment durations of 30 min and 60 min were employed to examine the dispersions of GNPs, according to [26]. After pre-mixing the cement and SP powder for 1 min at a low speed, the GNPs aqueous solutions were then added, followed by a 1-min high-speed mixing for enhanced dispersion. After a 1.5-min rest period to stabilize the mixture, a final 1-min high-speed mixing step was performed to ensure homogeneity.

(2) Mechanical stirring dispersion method

In this method, the SP and GNPs were first dispersed in water using a high-speed hand mixer for 3 min to achieve a uniform suspension. The resulting solution was then combined with cement and mixed using a planetary mixer to produce cement paste.

(3) Hybrid dispersion method with silica fume

To explore the synergistic effects between GNPs and SF, two SF dosages of 5% and 10% by weight of cement were selected [27]. The cement, GNPs, and SF were initially hand-mixed to achieve even distribution. Simultaneously, the SP was dissolved in water through manual stirring. Afterwards, the solution was then added, and the paste was mixed using a planetary mixer to complete the preparation process.

2.3 Testing methods

2.3.1 Fluidity test

The fluidity of the cement pastes was evaluated using a mini-slump test setup at ambient conditions. A hollow aluminum cylindrical mold, with an inner diameter of 30 mm and a height of 50 mm, was used. After mixing, fresh cement paste was immediately poured into the mold until slightly overfilled, and the surface was leveled. The mold was then carefully lifted vertically to allow the paste to spread freely and uniformly. The spread diameter of the paste was measured in two perpendicular directions, and the average value was recorded as the representative fluidity. Measurements were taken every 20 minutes over a 1-h period to evaluate the time-dependent flow behavior. Each fluidity test was performed at least twice to ensure data reliability.

2.3.2 Flexural strength test

The flexural strength tests were conducted on prism specimens with dimensions of 40 mm × 40 mm × 160 mm. The fresh cement paste was poured into the molds and allowed to set at room temperature for 24 hours before demolding. Subsequently, the specimens were cured in a standard curing room maintained at 25°C and 95% relative humidity until the designated testing ages (i.e., 3 days and 28 days).

The flexural strength was determined using a three-point bending method at a loading rate of 0.4 mm/min. The maximum applied load was recorded, and the

flexural strength (f_f, MPa) was calculated by:

$$f_f = \frac{3 \times P \times L}{2 \times W \times h^2}$$

where P is the maximum applied load (N), L is the support span length of the specimen (100 mm), W is the specimen width (40 mm), and h is the height of specimen (40 mm). The reported values represent the mean of duplicate measurements.

2.3.3 Compressive strength test

The broken specimens from the flexural tests were subsequently used for the evaluation of compressive strength. Tests were performed using a uniaxial compression testing machine under a constant loading rate of 2.40 kN/s until specimen failure. The final reported values of compressive strength were determined by taking the average of two test results.

2.3.4 Electrical resistivity test

The electrical resistivity of specimens at 28 days was quantified using the two-electrode method to minimize contact impedance [28]. As shown in Fig. 2, a DC regulated power supply paired with two Fluke 15B multimeters were used for the current and voltage measurements. The electrical resistivity (ρ, Ω·m) was calculated from two samples according to the following equation:

$$\rho = \frac{V \times W \times t}{I \times s}$$

where V is the voltage drop between probes (V), I is the applied current (A), W is the width of the specimen (40 mm), t is the specimen thickness (40 mm), s is the distance between probes (20 mm).

3. Results and discussion

3.1 Time–dependent fluidity

Fig. 3 illustrates the evolution of fluidity within the first hour after mixing for the cement pastes containing GNPs dispersed by different methods. It can be observed that all mixtures exhibited satisfactory initial workability, despite the low w/b ratio of 0.18 and the inclusion of GNPs. The initial fluidity was comparable among most groups, with the exception of the paste subjected to 60-min ultrasonication (i.e., 60min-ULT mixture), which displayed noticeably lower initial spread. This is possibly due to the enhanced dispersion of GNPs by the extended ultrasonic energy input, which breaks down the agglomerates more effectively, exposing a larger specific surface area and thereby raising the overall water demand. As GNPs interact with both SP molecules and cement particles, they can induce the formation of structured water layers and limit the amount of free water available for lubrication, leading to diminished initial flow.

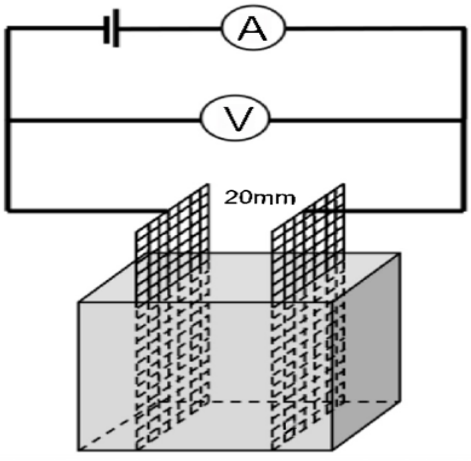

Fig. 2 Two-probe setup for electrical conductivity testing

With the evolution of elapsed time, all cement pastes experienced a progressive loss of fluidity, a common behavior in low-w/b cementitious suspensions. This reduction is primarily governed by ongoing hydration and pozzolanic reactions, which consume free water, promote the formation of C-S-H gel, and thus increase the viscosity of the paste. However, the rate and extent of this decline differed substantially among groups. The cement paste containing 10% SF exhibited the most pronounced decline in the fluidity. Unlike the ultrasonically treated samples, this reduction was not due to the improved GNP dispersion but rather to the intrinsic characteristics of silica fume [22], i.e., ultra-fine particle size, high specific surface area, and strong

pozzolanic reactivity. These properties increase the adsorption of SP molecules, reducing its dispersing efficiency and consequently lowering workability. In contrast, the 60min-ULT mixture exhibited a more moderate reduction. Although the enhanced dispersion initially elevated the water demand, the well-distributed GNPs likely contributed to a more stable and cohesive microstructure, slowing down the subsequent fluidity loss. By 60 minutes, its total reduction in fluidity was around 21%.

On the other hand, the paste prepared by mechanical stirring showed a more linear and continuous decline in fluidity. This behavior can be ascribed to the insufficient GNP dispersion, resulting in agglomeration that impedes flow, compounded by the gradual hydration-induced stiffening. At the end of the 60-min measurement period, the 10%SF mixture retained the lowest flowability, showing an overall reduction of approximately 29%. In contrast, the other cement pastes, despite the different reduction rates, converged to relatively similar final fluidity levels. This indicates that the dispersion techniques adopted in this study primarily affect the early-stage flow behavior rather than the long-term fluidity stability.

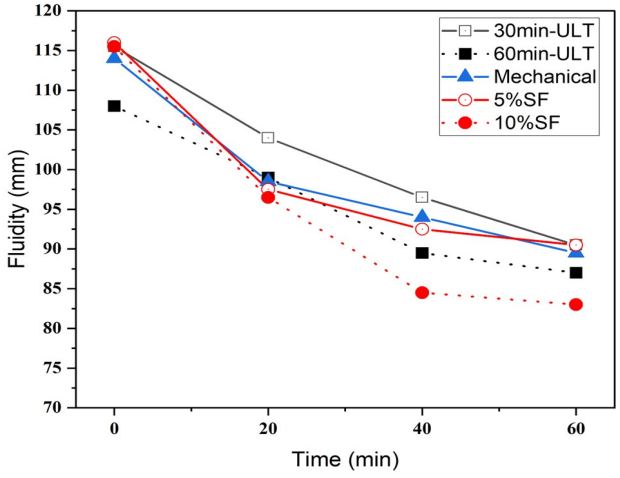

Fig. 3 Effect of GNP dispersion methods on the time-dependent fluidity of cement pastes

3.2 Mechanical properties

The comparisons of flexural and compressive strengths at 3 and 28 days for the studied cement pastes are presented in Fig. 4. Among all tested specimens, the 60min-ULT mixture demonstrated the highest flexural and compressive strengths at both 3 and 28 days. This enhancement can be possibly attributed to the superior dispersion achieved through extended ultrasonication, which enables the GNPs to function effectively as nanoscale reinforcement and nucleation sites for C-S-H growth. The well-distributed GNPs facilitate denser packing, reduce pore connectivity, and improve stress transfer at the microstructural level. The 10%SF mixture also exhibited notable improvements, particularly in early-age compressive strength, due to the synergistic effect of its high pozzolanic reactivity and particle-packing capability, which accelerate hydration and fill micro-voids within the matrix. In addition, the influence of silica fume was more pronounced in compressive than flexural performance. This reflects that the contribution of silica fume is primarily focused on the matrix densification rather than the nanoscale crack-bridging. Overall, the results demonstrate that both GNP dispersion quality and pozzolanic reaction significantly impact the mechanical performance of cement pastes.

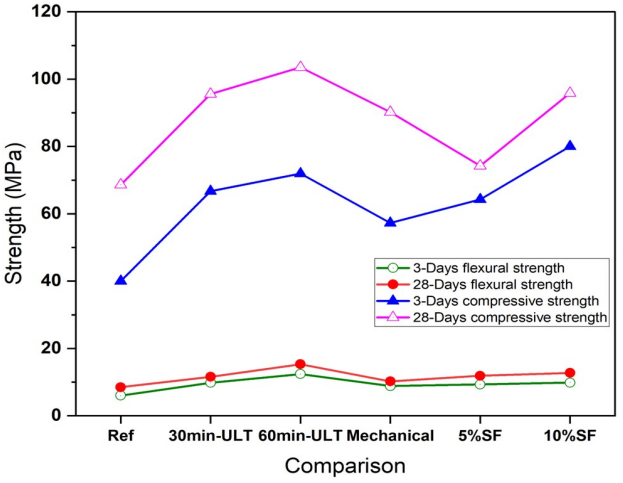

Fig. 4 Comparison of flexural and compressive strengths at 3 and 28 days

The incorporation of GNPs markedly affect cement hydration behavior, microstructural densification, and crack-bridging through three interconnected mechanisms [29, 30], including physical dispersion, chemical interaction, and microstructural evolution. The dispersion state governs the effective surface area of GNPs available for interaction with the cement matrix. Well-dispersed GNPs can establish a more

uniform network within the paste, promoting load transfer and forming potential conductive pathways. Conversely, inadequate dispersion results in particle agglomerations, which acts as weak zones and hinders stress distribution. The chemical interactions of GNPs involve nucleation and electrostatic adsorption of ions and SP molecules on their surfaces [31]. These interactions accelerate the precipitation of hydration products such as C-S-H gel and influence the ionic equilibrium in the pore solution. In addition, the microstructural evolution includes the progressive formation of C-S-H gel, the refinement of pore structure, and the modification of the interfacial transition zone (ITZ) between matrix and hydration products. The addition of GNPs enhances the structural compactness, reduces microcrack propagation, and provides a bridging effect across nanoscale voids, contributing to the higher overall strength. Collectively, these mechanisms influence the compressive strength, flexural behavior, and electrical resistivity, which will be discussed in detail below.

3.2.1 Flexural strength

The flexural strength at 3 days and 28 days for the cement pastes incorporating GNPs and prepared using different dispersion methods are presented in Fig. 5. At 3 days, all GNPs-containing samples exhibited significant improvements in flexural strength compared with the reference paste. Notably, the 60min-ULT mixture showed the greatest enhancement, with its flexural strength nearly doubled that of the reference paste. This is possibly attributed to the excellent dispersion of GNPs, which promotes effective crack-bridging and stress-transfer mechanisms even in the immature cement matrix [32]. The uniformly distributed GNPs form a continuous reinforcing network that restrains early microcrack development and facilitates load redistribution across the matrix, as schematically illustrated in Fig. 6. By contrast, the 15%SF and 30min-ULT mixtures displayed similar improvements in the flexural strength, showing an approx. 64% increase over the reference paste. Meanwhile, the 5%SF and mechanical stirring pastes exhibited more modest gains of 55% and 47%, respectively.

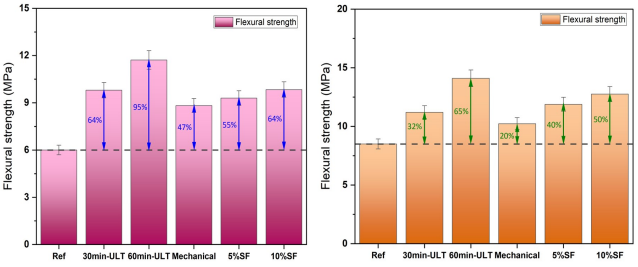

Fig. 5 Flexural strength of the studied cement pastes

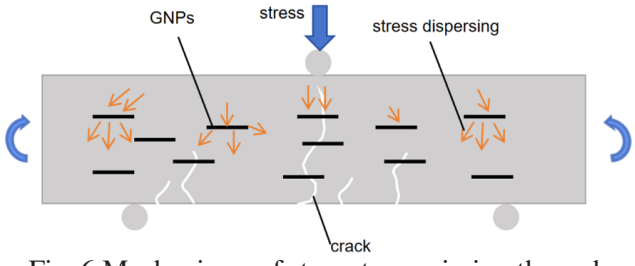

Fig. 6 Mechanisms of stress transmission through GNPs in cement matrix

At 28 days, the relative improvement in flexural strength due to GNP incorporation was slightly reduced compared with the early-age results. Nonetheless, the 60min-ULT mixture continued to exhibit the highest flexural strength, achieving a 65% increase over the reference paste. This result confirms that well-dispersed GNPs maintain strong interfacial bonding with hydration products, sustaining efficient load transfer and crack-bridging over time. Besides, the dispersion achieved by prolonged ultrasonication remains effective throughout the whole hydration process, supporting both early and long-term reinforcement. The 10%SF mixture also demonstrated substantial flexural strength enhancement with approx. 50% higher than the reference. This is possibly due to the refinement of pore structure through pozzolanic reactions of silica fume, although their effect is less pronounced than that of prolonged ultrasonication.

In contrast, the samples prepared by mechanical stirring showed minimal improvement of 20% compared to the reference paste. The inadequate dispersion of GNPs and silica fume likely caused agglomeration and nonuniform particle distribution. In this case, GNPs are entrapped within dense clusters of silica fume particles, which isolates them from interacting effectively with the surrounding cementitious matrix, as schematically illustrated in

Fig. 7. As a result, these localized agglomerates limit the ability of GNPs to act as nucleation sites, reducing the formation of hydration products in those regions. The presence of these inhomogeneous "island" zones weakens the interfacial bonding, thereby decreasing the reinforcing effect of GNPs and ultimately limiting gains in the mechanical properties. In addition, the reduced improvements in the flexural strength at 28 days for the 5%SF and 30min-ULT mixtures to a certain extent confirm that the insufficient GNP dispersion may limit the strength development beyond early ages.

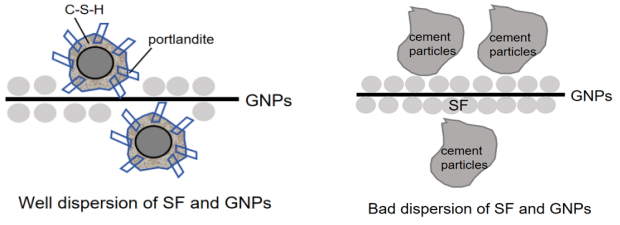

Fig. 7 Mechanism of silica fume and GNPs dispersion in cement paste

3.2.2 Compressive strength

The compressive strength results of cement pastes incorporating GNPs under different dispersion methods are presented in Fig. 8. The results indicate that the combination of GNPs and 10% silica fume achieved the highest 3-day compressive strength, with an approximately 100% increase relative to the reference paste. This possibly arises from the synergistic effects between GNPs and silica fume. The high pozzolanic reactivity of silica fume promotes the formation of additional C-S-H gel during the secondary hydration reactions, thereby densifying the microstructure and enhancing bonding strength [33]. Furthermore, its ultrafine particle size enables a pronounced micro-filling effect, where silica fume particles occupy voids between cement grains and optimize the overall particle packing [34]. This effect is particularly beneficial in low w/b cementitious systems adopted in this study, where limited free water maximizes the advantages of enhanced packing density and refined pore structure. The 60min-ULT mixture ranked the second, achieving an 80% increase in 3-day compressive strength, followed by the 30min-ULT cement paste with a 67% improvement, emphasizing the role of dispersion quality in achieving effective load-bearing reinforcement.

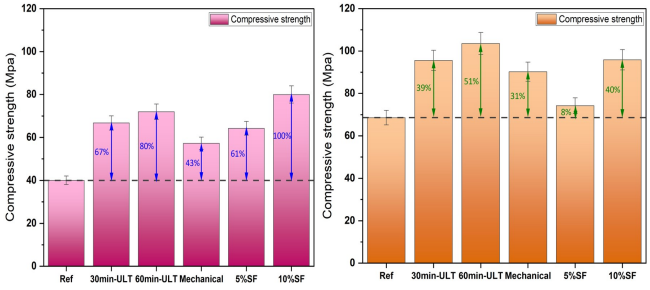

Fig. 8 Compressive strength of the studied cement pastes

At 28 days, the 60min-ULT mixture surpassed all other pastes, showing a 51% increase in compressive strength compared with the reference sample. This is closely related to the stability and uniformity of GNP dispersion achieved through prolonged ultrasonication. The well-dispersed GNPs serve as nucleation sites for C-S-H formation, accelerating hydration kinetics and promoting the development of a finer and denser microstructure over time. The sustained nucleation effect leads to a cumulative increase in the degree of hydration, thereby improving matrix compactness and strength after 28 days of curing. The 10%SF mixture maintained a 40% improvement over the reference, while the 30min-ULT and 5%SF samples showed moderate increases of 31% and 8%, respectively. These findings are consistent with prior research demonstrating that well-dispersed GNPs play a dominant role in enhancing the long-term mechanical properties of cementitious composites [35].

The difference in compressive strength between 60-min and 30-min treatments (approx. 20%) highlights the critical influence of ultrasonication duration on achieving stable dispersion of GNPs. With the increase of ultrasonication time, the repeated formation and collapse of microbubbles produce localized high-pressure and high-shear zones, effectively overcoming the van der Waals forces between graphene layers. This is beneficial to the deagglomeration of GNPs. As a result, GNPs are more uniformly distributed in cement matrix, forming continuous reinforcement pathways and thus contributing to porosity reduction and ITZ strengthening. In contrast, specimens prepared by mechanical stirring exhibited the lowest compressive

strength among all groups. The insufficient energy fails to disrupt GNP agglomerates, resulting in non-uniform dispersion and the formation of weak zones where stress concentrations develop under load. Instead of reinforcing the matrix, these agglomerates act as defects, thereby negating the potential benefits of GNP incorporation.

3.3 Electrical conductivity

The 28-day electrical resistivity results of cement pastes incorporating GNPs dispersed by different methods are presented in Fig. 9. The results clearly demonstrate that the dispersion method strongly influences the electrical properties of GNPs-reinforced cement composites. The 60min-ULT mixture exhibited the lowest electrical resistivity, with a reduction of 28.82% compared with the reference paste, followed by the 30min-ULT and mechanical stirred groups. In contrast, the incorporation of silica fume markedly increased electrical resistivity, exhibiting a clear concentration-dependent trend. The addition of 5% and 10% silica fume led to dramatic resistivity increases of 344.7% and 641.4%, respectively. This reflects the negative influence of silica fume on the conductive network compared to the physical dispersion methods. Similar observations have been reported in previous studies [36-38], where improved GNP dispersion promoted network percolation and reduced contact resistance between nanosheets.

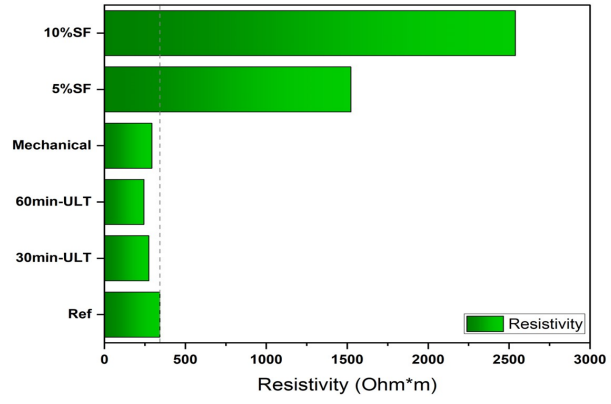

Fig. 9 Electrical resistivity of cement pastes at 28 days

The electrical conduction in cementitious materials occurs primarily via two mechanisms [39], i.e., ionic conduction, governed by ion transport within the pore solution, and electronic conduction, arising from interconnected conductive networks such as carbon-based additives. In GNPs-modified pastes, both mechanisms coexist, and their relative contribution depends strongly on the dispersion of GNPs and the resulting microstructural continuity. For well-dispersed systems, ions migrate through the pore solution while electrons transfer along percolated GNPs pathways embedded within the cement matrix. Prolonged ultrasonication enhances the uniform distribution of GNPs, allowing them to form continuous conductive bridges across cement matrix. This interconnected microstructure provides efficient electron transport routes, significantly lowering concrete resistivity.

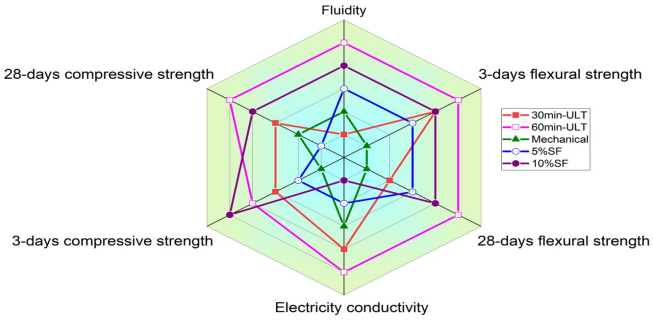

Fig. 10 Comprehensive performance evaluation of different dispersion methods

By contrast, the native influence of silica fume on the electrical resistivity can be attributed to several factors. The micro-filling effect of silica fume refines the pore structure and reduces pore connectivity, hindering ionic mobility and thereby elevating the resistivity. Its pozzolanic reaction consumes $Ca(OH)_5$ and forms additional C-S-H gel, which further densifies the matrix. This reaction also lowers the alkalinity and ion concentration of the pore solution, diminishing the ionic component of conductivity. Furthermore, silica fume particles physically separate GNPs, interrupting the continuity of conductive pathways. As a result, the paste system shift from a percolating to a non-percolating state, leading to a sharp increase in electrical resistivity. In a word, the ultrasonic dispersion and silica fume incorporation exert opposite effects on the electrical performance of GNPs-containing cement composites. This arises from the complex interactions among the dispersion quality of GNPs, pore structure, and ionic composition of the pore solution, which together govern the conductive

behavior of the composites.

To evaluate the influence of different dispersion methods, all the measured performance indicators, including fluidity, mechanical strength, and electrical conductivity were normalized and ranked into five performance levels, as illustrated in Fig. 10. It can be observed that the 60-min ultrasonication method achieved the most balanced and superior overall performance, indicating the optimal utilization of GNPs and microstructural synergy. Consequently, ultrasonically dispersed GNP composites are promising for multifunctional applications, such as self-sensing, structural health monitoring, and electromagnetic shielding. By contrast, the 10%SF mixture exhibited a strength enhancement but poor electrical conductivity possibly due to the excessive microstructural densification and disruption of the conductive network. These characteristics make silica fume-modified GNPs-containing cementitious composites ideal for corrosion-resistant coatings, impermeable layers, and insulating applications where mechanical properties and durability are prioritized.

3.4 Microstructure and hydration products

Fig. 11 shows representative SEM images of reference and 60min-ULT mixtures after the compressive tests. The observations reveal distinct microstructural differences among the paste samples. In particular, no further hydration products are observed in the cracks of the reference paste. By contrast, the 60min-ULT paste exhibits a compact morphology characterized by well-distributed graphene nanoplatelets effectively bridging microcracks and voids within the matrix. The nucleation effect of well-dispersed GNPs provides additional nucleation sites for the growth of hydration products, accelerating early hydration reactions and promoting a finer and more continuous microstructure. This bridging mechanism serves as a critical contributor to the enhanced mechanical performance, as GNPs impede crack initiation and propagation while redistributing localized stresses throughout the composite [32]. This is in good agreement with the flexural strength in Fig. 5. The SEM observations reveal that extended ultrasonication treatment not only breaks down agglomerates but also promotes uniform dispersion of GNPs, enabling a homogeneous reinforcement network that enhances both structural integrity and electrical resistivity.

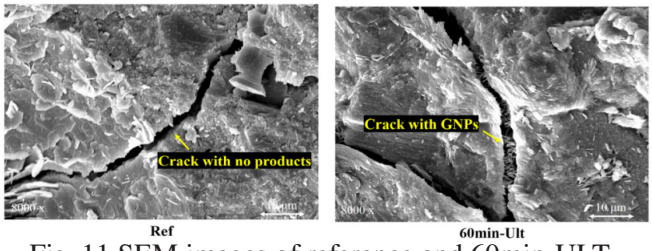

Fig. 11 SEM images of reference and 60min-ULT mixtures

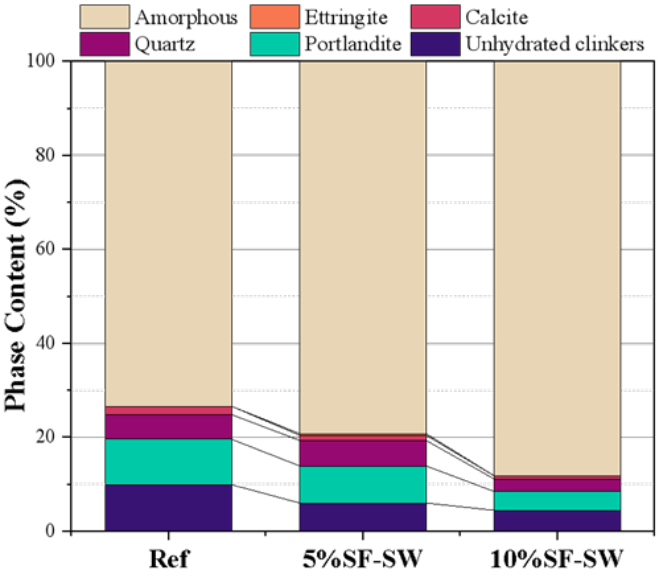

Fig. 12 Phase composition determined by Quantitative-XRD

The phase composition determined by quantitative-XRD analysis for the reference and the silica fume incorporation mixtures is presented in Fig. 12. The relative proportions of unhydrated clinker phases (C_3S, C_2S) and amorphous phases (primarily C-S-H) were used as indicators of hydration progression. As can be seen from Fig. 12, the mixtures containing silica fume exhibited a pronounced reduction in portlandite content accompanied by an increase in amorphous C-S-H. This transformation results from the pozzolanic reaction between reactive silica and calcium hydroxide, producing additional C-S-H gels that fills capillary

pores, refines the microstructure, and strengthens the ITZ in the paste matrix. This directly contributes to the improved compressive strength and reduced permeability. The quantitative-XRD results further substantiate the SEM microstructural findings by revealing distinct differences in the hydration degree and phase content among the various mixtures.

Overall, the microstructural and phase analyses confirm that the degree of GNP dispersion directly governs the balance between mechanical reinforcement and electrical conductivity. Extended ultrasonication produces a well-integrated microstructure capable of simultaneously enhancing strength, toughness, and conductivity, whereas the addition of silica fume promotes the structure densification at the expense of electrical performance.

4.Conclusion

This study examined the influence of graphene nanoplatelets (GNPs) dispersion methods on the flowability, mechanical, and electrical properties of ultra-low-w/b cementitious pastes. Based on the experimental findings, the following key conclusions can be drawn:

(1) Ultrasonic treatment significantly enhances both the mechanical properties and electrical conductivity of GNPs-containing cementitious composites, with flexural and compressive strengths increasing by 65% and 51% and resistivity reducing by nearly 29% after 28 days, respectively. This is possibly due to the uniform dispersion of GNPs and the formation of continuous percolation networks within the cement matrix.

(2) The incorporation of silica fume primarily improves the early compressive strength while substantially increasing the electrical resistivity up to 641%. This can be attributed to the high pozzolanic reactivity and micro-filling effects of ultra-fine silica fume particles, which densifies the microstructure and disrupts the conductive pathways.

(3) Based on the findings in this study, the optimal dispersion strategy depends on the intended balance between mechanical properties and electrical conductivity. Ultrasonic dispersion is recommended when functional conductivity and sensing capability are desired, whereas silica fume addition is preferable for enhanced durability and chemical resistance.

Future research should further explore the multiscale interactions between GNPs, mineral admixtures, and hydration products to better elucidate the mechanisms governing conductivity and mechanical enhancement in ultra-low-w/b systems. In addition, long-term performance under realistic environmental conditions, such as chloride exposure and sustained loading, warrants systematic investigation to assess the practical applicability of GNPs-modified UHPC in smart infrastructure.

CRediT authorship contribution statement

Dengwu Jiao: Writing – review & editing, Supervision, Project administration, Methodology, Funding acquisition, Conceptualization.

Shuo Wang: Writing – original draft, Methodology, Investigation, Formal analysis, Conceptualization.

Feng Hu: Writing – original draft, Investigation.

Declaration of Competing Interest

The authors declare that they have no known competing financial interests or personal relationships that could have appeared to influence the work reported in this paper.

Acknowledgments

The authors gratefully acknowledge the financial support from the National Natural Science Foundation of China (52408295), the Guangdong Basic and Applied Basic Research Foundation (2025A1515012809), the Environment and Conservation Fund (No. 04/2023), and the Early Career Scheme (ECS) from the Research Grants Council of Hong Kong SAR (21211024).

Reference

[1] C.R. Gagg, Cement and concrete as an engineering material: An historic appraisal and case study analysis, Engineering Failure Analysis, 2014, 40: 114-140.

[2] M. Chemrouk, The deteriorations of reinforced concrete and the option of high performances reinforced concrete, Procedia Engineering, 2015, 125: 713-724.

[3] M. Liu, J. Li, D. Jiao, et al., Micromechanical Prediction of the Flexural Behavior of Self-Compacting Ultra-High Performance Concrete (SC-UHPC), Structures, 2025, 80: 109828.

[4] F. Sanchez, K. Sobolev, Nanotechnology in concrete–a review, Construction and building materials, 2010, 24(11): 2060-2071.

[5] H.N.C. Change, How nanotechnology can change the concrete world, American Ceramic Society Bulletin, 2005, 84(11): 17.

[6] Y. Lin, H. Du, Graphene reinforced cement composites: A review, Construction and Building Materials, 2020, 265: 120312.

[7] W. Dong, Y. Huang, B. Lehane, et al., Mechanical and electrical properties of concrete incorporating an iron-particle contained nano-graphite by-product, Construction and Building Materials, 2021, 270: 121377.

[8] X. Huang, Z. Yin, S. Wu, et al., Graphene$_5$ based materials: synthesis, characterization, properties, and applications, small, 2011, 7(14): 1876-1902.

[9] Q. Zheng, B. Han, X. Cui, et al., Graphene-engineered cementitious composites: Small makes a big impact, Nanomaterials and Nanotechnology, 2017, 7: 1847980417742304.

[10] S. Qamar, N. Ramzan, W. Aleem, Graphene dispersion, functionalization techniques and applications: A review, Synthetic Metals, 2024, 307: 117697.

[11] B. Wang, B. Pang, Mechanical property and toughening mechanism of water reducing agents modified graphene nanoplatelets reinforced cement composites, Construction and Building Materials, 2019, 226: 699-711.

[12] Z. Jiang, O. Sevim, O.E. Ozbulut, Mechanical properties of graphene nanoplatelets-reinforced concrete prepared with different dispersion techniques, Construction and Building Materials, 2021, 303: 124472.

[13] E. Elbatanouny, L. Ai, E. Deaver, et al., Impact of graphene on microstructure and compressive strength of cement mortars utilizing two different dispersion methods, Practice Periodical on Structural Design and Construction, 2024, 29(1): 04023065.

[14] T. Piao, P. Li, S. Im, et al., Impacts of graphene nanoribbon dispersion and stability on the mechanical and hydration properties of cement paste: Insights from surfactant-assisted ultrasonication, Journal of Building Engineering, 2024, 96: 110469.

[15] V.U. Siddiqui, S. Sapuan, M.R. Hassan, Innovative dispersion techniques of graphene nanoplatelets (GNPs) through mechanical stirring and ultrasonication: Impact on morphological, mechanical, and thermal properties of epoxy nanocomposites, Defence Technology, 2025, 43: 13-25.

[16] D. Jiao, C. Shi, Q. Yuan, et al., Effect of constituents on rheological properties of fresh concrete-A review, Cement and concrete composites, 2017, 83: 146-159.

[17] Y. Mao, D. Jiao, X. Hu, et al., Dispersion behavior of silica fume in cementitious suspensions, Cement and Concrete Composites, 2024, 151: 105605.

[18] Y. Mao, D. Jiao, X. Hu, et al., Effect of dispersion behavior of silica fume on the rheological properties and early hydration characteristics of ultra-high strength mortar, Cement and Concrete Composites, 2024, 152: 105654.

[19] N.M. Azmee, N. Shafiq, Ultra-high performance concrete: From fundamental to applications, Case Studies in Construction Materials, 2018, 9: e00197.
[20] M. Zhou, W. Lu, J. Song, et al., Application of ultra-high performance concrete in bridge engineering, Construction and Building Materials, 2018, 186: 1256-1267.
[21] M. Bajaber, I. Hakeem, UHPC evolution, development, and utilization in construction: A review, Journal of Materials Research and Technology, 2021, 10: 1058-1074.
[22] X. Li, A.H. Korayem, C. Li, et al., Incorporation of graphene oxide and silica fume into cement paste: A study of dispersion and compressive strength, Construction and Building Materials, 2016, 123: 327-335.
[23] Z. Lu, D. Hou, A. Hanif, et al., Comparative evaluation on the dispersion and stability of graphene oxide in water and cement pore solution by incorporating silica fume, Cement and Concrete Composites, 2018, 94: 33-42.
[24] C. Shi, Z. Wu, J. Xiao, et al., A review on ultra high performance concrete: Part I. Raw materials and mixture design, Construction and Building Materials, 2015, 101: 741-751.
[25] O. Mishra, S. Singh, An overview of microstructural and material properties of ultra-high-performance concrete, Journal of Sustainable Cement-Based Materials, 2019, 8(2): 97-143.
[26] M. Sandhya, D. Ramasamy, K. Sudhakar, et al., Ultrasonication an intensifying tool for preparation of stable nanofluids and study the time influence on distinct properties of graphene nanofluids–A systematic overview, Ultrasonics sonochemistry, 2021, 73: 105479.
[27] Y. Liu, C. Shi, Z. Zhang, et al., Mechanical and fracture properties of ultra-high performance geopolymer concrete: Effects of steel fiber and silica fume, Cement and Concrete Composites, 2020, 112: 103665.
[28] S. Bai, L. Jiang, N. Xu, et al., Enhancement of mechanical and electrical properties of graphene/cement composite due to improved dispersion of graphene by addition of silica fume, Construction and Building Materials, 2018, 164: 433-441.
[29] A.G. Alex, A. Kedir, T.G. Tewele, Review on effects of graphene oxide on mechanical and microstructure of cement-based materials, Construction and Building Materials, 2022, 360: 129609.
[30] S. Lv, Y. Ma, C. Qiu, et al., Effect of graphene oxide nanosheets of microstructure and mechanical properties of cement composites, Construction and building materials, 2013, 49: 121-127.
[31] W. Baomin, D. Shuang, Effect and mechanism of graphene nanoplatelets on hydration reaction, mechanical properties and microstructure of cement composites, Construction and Building Materials, 2019, 228: 116720.
[32] C. Massion, Y. Lu, D. Crandall, et al., Graphene nanoplatelets reinforced cement as a solution to leaky wellbores reinforcing weak points in hydrated Portland cement with graphene nanoparticles improves mechanical and chemical durability of wellbore cements, Cement and Concrete Composites, 2022, 133: 104726.
[33] A. Muller, K. Scrivener, J. Skibsted, et al., Influence of silica fume on the microstructure of cement pastes: New insights from 1H NMR relaxometry, Cement and Concrete Research, 2015, 74: 116-125.
[34] Z. Zhang, B. Zhang, P. Yan, Comparative study of effect of raw and densified silica fume in the paste, mortar and concrete, Construction and Building Materials, 2016, 105: 82-93.
[35] H. Du, S. Dai Pang, Dispersion and stability of graphene nanoplatelet in water and its

influence on cement composites, Construction and Building Materials, 2018, 167: 403-413.
[36] S.-J. Lee, I. You, S. Kim, et al., Self-sensing capacity of ultra-high-performance fiber-reinforced concrete containing conductive powders in tension, Cement and Concrete Composites, 2022, 125: 104331.
[37] J.-L. Le, H. Du, S. Dai Pang, Use of 2D Graphene Nanoplatelets (GNP) in cement composites for structural health evaluation, Composites Part B: Engineering, 2014, 67: 555-563.
[38] S. Sun, B. Han, S. Jiang, et al., Nano graphite platelets-enabled piezoresistive cementitious composites for structural health monitoring, Construction and Building Materials, 2017, 136: 314-328.
[39] B. Han, S. Ding, X. Yu, Intrinsic self-sensing concrete and structures: A review, Measurement, 2015, 59: 110-128.